Journal of Sound and Vibration (2002) **255**(2), 203–228
doi:10.1006/jsvi.2001.4150, available online at http://www.idealibrary.com on IDEAL®

DSC ANALYSIS OF RECTANGULAR PLATES WITH NON-UNIFORM BOUNDARY CONDITIONS

Y. B. Zhao and G. W. Wei

Department of Computational Science, Faculty of Science, National University of Singapore, Singapore 117543, *Singapore. E-mail: cscweigw@nus.edu.sg*

(*Received* 17 *July* 2000, *and in final form* 11 *July* 2001)

This paper introduces the discrete singular convolution (DSC) for the vibration analysis of rectangular plates with non-uniform and combined boundary conditions. A systematic scheme is proposed for the treatment of boundary conditions required in the proposed approach. The validity of the DSC approach for plate vibration is tested by using a large number of numerical examples that have a combination of simply supported, clamped and transversely supported (with non-uniform elastic rotational restraint) edges. The present results are in excellent agreement with those in the literature.

1. INTRODUCTION

Plates, beams, frames and shells are basic elements for structural analysis and are of great practical significance to civil, mechanical, and aerospace engineerings. Apart from a few analytically solvable cases, there is no general solution for the static analysis of structures, and, therefore, numerical simulation is one of the major approaches. The performance of a numerical simulation depends crucially on the computational method employed. Typically, structural analysis computations are accomplished by using either global methods [1–5] or local methods [6–15]. Global methods are highly accurate but are cumbersome to implement in complex geometries and non-conventional boundary conditions. For example, a global method may be found to converge slowly due to a mixed boundary condition which induces a large local stress concentration. In contrast, local methods are easy to implement for complex geometries and discontinuous boundary conditions. However, the accuracy of local methods is usually very low. For example, it may have convergence problems for the prediction of large eigenvalues in a vibration analysis.

The vibration analysis of rectangular plates with various uniform and non-uniform boundary conditions has received considerable attention. Most results are well documented in Leissa's book [16]. A variety of computational methods have been employed successfully for such analysis. These include the Rayleigh method [17], Ritz variational methods [18, 19], methods of finite strip [20, 21] and spline finite strip [22], the series expansion [23] for orthotropic plates, methods of differential quadrature [24] and generalized differential quadrature [25, 26], etc. However, alternative approaches might provide better results for plate analysis. In fact, many difficult problems that involve singularities require an improvement in computational methodology.

Recently, a discrete singular convolution (DSC) algorithm was proposed as a potential approach for the computer realization of singular convolutions [27, 28]. Sequences of approximations to the singular kernels of Hilbert type, Abel type and delta type were

0022-460X/02/$35.00

constructed. Applications to analytical signal processing, Radon transform and surface interpolation were discussed. The mathematical foundation of this algorithm is the theory of distributions [29]. Numerical solutions to differential equations are formulated via the singular kernels of the delta type. By appropriately selecting the parameters of a DSC kernel, the DSC approach exhibits global methods' accuracy for integration and local methods' flexibility for handling complex geometries and boundary conditions. Based on the DSC framework, a unification was discussed for a number of conventional computational methods, including global, local, Galerkin, collocation, and finite difference methods [28].

Many DSC kernels, such as (regularized) Shannon's delta kernel, (regularized) Dirichlet kernel, (regularized) Lagrange kernel and (regularized) de la Vallée Poussin kernel, have been constructed [27]. Practical applications were examined for the numerical solution of the Fokker–Planck equation [27] of statistical theory and for the Schrödinger equation [30] of quantum mechanics. Another development in the application of the DSC algorithm is its use in computing numerical solutions of the Navier–Stokes equation. The standard Taylor problem (2-D incompressible Navier–Stokes equation with periodic boundary conditions) was solved to machine precision with a few grid points [31]. Most recently, the DSC algorithm was used to resolve a few challenging problems. It was utilized to integrate the (non-linear) sine-Gordon equation with the initial values close to a homoclinic manifold singularity [32], for which conventional local methods encounter great difficulties and result in numerically induced chaos [33]. Another complex example that was resolved by using the DSC algorithm is the integration of the (non-linear) Cahn–Hilliard equation in a circular domain, which is challenging because of the fourth order artificial singularity at the origin and the complex phase-space geometry [34].

Further development, which is of relevance to the present work is the use of the DSC algorithm in structural analysis. Previous work has shown that the DSC approach provided more than 10 significant figure accuracy for the first 100 eigenmodes of a rectangular plate vibration with simply supported boundary conditions [31, 35]. The vibration of circular plates was also analyzed with clamped boundary conditions [31]. Extremely accurate DSC results were obtained for beam bending, vibration and buckling [36, 37]. However, the boundary conditions of the previous work are relatively simple and uniform. In the earlier investigation, it was not clear as to how the DSC algorithm could be implemented in the analysis of plates with non-uniform boundary conditions. In particular, the implementation is non-trivial if the plates are transversely supported with non-uniform elastic rotational restraint [26].

The purpose of this study is to introduce the DSC algorithm for the analysis of rectangular plates with non-uniform and combined boundary conditions. A new unified scheme is proposed for treating all three boundary conditions. We demonstrate the usefulness and reliability of the present approach for vibration analysis by analyzing plates with 21 distinct configurations, which comprise all the possible combinations of three boundary conditions, viz., simply supported, clamped and transversely supported with non-uniform elastic rotational restraint edges.

This paper is organized as follows: In section 2, we describe the theory and algorithm for vibration analysis used in the present study. The theory of discrete singular convolution is briefly reviewed. A number of DSC kernels are constructed. A unified scheme is presented for the treatment of all three boundary conditions. The application of this algorithm to plate vibration with various boundary conditions is given in section 3. The utility and robustness of the proposed method is illustrated by a large number of numerical experiments. This paper ends with a conclusion.

2. THEORY AND ALGORITHM

2.1. APPROXIMATION OF SINGULAR CONVOLUTION

Singular convolutions (SC) are a special class of mathematical transformations, which appear in many science and engineering problems, such as the Hilbert, Abel and Radon transforms. It is the most convenient way to discuss the singular convolution in the context of the theory of distributions. The latter has important effects in mathematical analysis. It not only provides a rigorous justification for a number of informal manipulations in physical science and engineering, but also opens a new area of mathematics, which in turn gives impetus in many other mathematical disciplines, such as operator calculus, differential equations, functional analysis, harmonic analysis and transformation theory. In fact, the theory of wavelets and frames, a new mathematical branch developed in recent years, can also find its root in the theory of distributions.

Let T be a distribution and $\eta(x)$ be an element of the space of test functions. A singular convolution can be defined as

$$F(t) = (T * \eta)(t) = \int_{-\infty}^{\infty} T(t - x)\eta(x)\,\mathrm{d}x, \tag{1}$$

where $T(t - x)$ is a *singular kernel*. Depending on the form of the kernel T, the singular convolution is the central issue for a wide range of science and engineering problems. For example, kernel $T(x) = 1/x$ occurs commonly in the spectral properties of time correlation functions, electrodynamics, linear response theory, analytic signal processing and the theory of analytic functions. Kernel $T(x) = 1/x^2$ is widely utilized in tomography. Both the kernels belong to the family of *Hilbert type* kernels that have the following general form:

$$T(x) = \frac{1}{x^n} \quad (n = 1, 2 \cdots). \tag{2}$$

Of particular relevance to the present study are the singular kernels of *delta* type

$$T(x) = \delta^{(n)}(x) \quad (n = 0, 1, 2, \ldots), \tag{3}$$

where δ is the delta distribution and the superscript denotes the nth order distribution derivative. Although the delta distribution is called the Dirac delta function, it is not a function. In fact, it does not even have a value anywhere. Mathematically, $\delta^{(n)}(x)$ are distributions with point support and can be classified as elements of the Sobolev space of negative order H^{α}, $(\alpha = -1, -2, \cdots)$. The kernel $T(x) = \delta^{(0)}(x)$ is important for interpolation and $T(x) = \delta^{(n)}(x)$, $(n = 1, 2, \ldots)$ are essential for differentiations. However, these kernels cannot be applied directly in digital computations because of their singular character. A solution of this is to construct an approximation kernel $\{T_{\alpha}\}$ such that it converges to the singular kernel under the condition

$$\lim_{\alpha \to \alpha_0} T_{\alpha} \to T(x), \tag{4}$$

where α_0 is a generalized limit. In the case of $T(x) = \delta(x)$, the kernel $T_{\alpha}(x)$ is called a delta sequence kernel. With a sufficiently smooth approximation, it makes sense to consider a discrete singular convolution.

$$F_{\alpha}(t) = \sum_{k} T_{\alpha}(t - x_k) f(x_k), \tag{5}$$

where $F_\alpha(t)$ is an approximation of $F(t)$ and $\{x_k\}$ is an appropriate set of discrete points on which the DSC is well defined. Here, in general, $f(x)$ is not required to be a test function. The singular kernel of Hilbert type was described in reference [27]. For the solution of differential equations, only the DSC kernels of the delta type are required. Hence, in the rest of the paper, we focus our attention to the DSC kernels of the delta type and use a few examples to illustrate the algorithm.

Example 1. *Dirichlet's delta kernel.* One of the most important examples of the DSC kernels is Dirichlet's delta kernel

$$\delta_\alpha(x) = \begin{cases} D_\alpha(x) & \text{for } |x| \leqslant \pi \quad \text{for } \alpha = 0, 1, 2, \dots, \\ 0 & \text{otherwise,} \end{cases} \tag{6}$$

where D_α is the Dirichlet kernel which is defined as

$$\begin{aligned} D_\alpha(x) &= \frac{1}{\pi}\left[\frac{1}{2} + \cos(x) + \cos(2x) + \cdots + \cos(\alpha x)\right] \\ &= \frac{\sin[(\alpha + \frac{1}{2})x]}{2\pi \sin(\frac{1}{2}x)}, \quad \alpha = 0, 1, 2, \dots . \end{aligned} \tag{7}$$

Dirichlet's delta kernel plays an important role in approximation theory and is the key element in trigonometric polynomial approximations. Physically, it arises from the Fourier optics and describes the diffraction light passing a regular array of pinholes in which the kth pinhole's contribution is proportional to e^{ik}. It also has important application in the representation theory of continuous rotational group.

Example 2. *Modified Dirichlet's delta kernel.* From the point of view of approximation theory, sometimes there is some advantage in taking the last term in D_α with a factor of $\frac{1}{2}$. Hence, the modified Dirichlet kernel is given by

$$\begin{aligned} D_\alpha^*(x) &= D_\alpha - \frac{1}{2\pi}\cos(\alpha x) \\ &= \frac{\sin(\alpha x)}{2\pi \tan(\frac{1}{6}x)}, \quad \alpha = 0, 1, 2, \dots . \end{aligned} \tag{8}$$

Obviously, over the range $(-\pi, \pi)$, the difference $D_\alpha - D_\alpha^*$ is very small when α is large enough, that is

$$\lim_{\alpha \to \infty} D_\alpha^* \to D_\alpha. \tag{9}$$

Both the Dirichlet kernel and the modified Dirichlet kernel are equivalent with respect to convergence.

The expression

$$\delta_\alpha(x) = \begin{cases} D_\alpha^*(x) & \text{for } |x| \leqslant \pi \quad \text{for } \alpha = 0, 1, 2, \dots, \\ 0 & \text{otherwise} \end{cases} \tag{10}$$

gives a delta sequence of the Dirichlet type as $\alpha \to \infty$.

Example 3. *The de la Vallée Poussin kernel.* The de la Vallée Poussin kernel is given by

$$\begin{aligned} P_{n,p}(x) &= \frac{1}{p+1}\sum_{k=n-p}^{p} D_k(x) \\ &= \frac{1}{2\pi} + \frac{1}{\pi}\sum_{k=1}^{n-p}\cos(kx) + \frac{1}{\pi}\sum_{k=1}^{p}\left[1 - \frac{k}{p+1}\right]\cos[(n-p+k)x] \\ &= \frac{\sin[(2n+1-p)x/2]\sin[(p+1)x/2]}{2\pi(p+1)\sin^2(x/2)}, \quad p = 0, \ldots, n;\ n = 0, 1, \ldots, \end{aligned} \tag{11}$$

where $D_k(x)$ are Dirichlet kernels given by equation (7). It is interesting to note that the de la Vallée Poussin kernels reduce to Ferér's positive definite kernels (which are different from the kernels of Dirichlet type) when $p = n$. The de la Vallée Poussin delta sequence is given by

$$\delta_{n,p}(x) = \begin{cases} P^*_{n,p}(x) & \text{for } |x| \leqslant \pi \quad \text{for } p = 0, \ldots, n;\ n = 0, 1, \ldots, \\ 0 & \text{otherwise} \end{cases} \tag{12}$$

as $n, p \to \infty$. Obviously, the de la Vallée Poussin delta sequence is of the Dirichlet type when $p < n$.

Numerically, a very useful form of the simplified de la Vallée Poussin kernel can be given by

$$\delta_\alpha(x) = \frac{1}{\pi\alpha}\frac{\cos(\alpha x) - \cos(2\alpha x)}{x^2}. \tag{13}$$

Example 4. *Shannon's delta sequence.* Shannon's delta kernel (or Dirichlet's continuous delta kernel) is given by the following (inverse) Fourier transform of the characteristic function, $\chi_{[-\alpha/(2\pi),\,\alpha/(2\pi)]}$,

$$\begin{aligned} \delta_\alpha(x) &= \int_{-\infty}^{\infty} \chi_{[-\alpha/(2\pi),\,\alpha/(2\pi)]} \mathrm{e}^{-\mathrm{i}2\pi\xi x}\,\mathrm{d}\xi \\ &= \frac{\sin(\alpha x)}{\pi x}. \end{aligned} \tag{14}$$

Alternatively, Shannon's delta kernel can be given as an integration

$$\delta_\alpha(x) = \frac{1}{\pi}\int_0^\alpha \cos(xy)\,\mathrm{d}y \tag{15}$$

or as the limit of a continuous product

$$\delta_\alpha(x) = \lim_{N\to\infty}\frac{\alpha}{\pi}\prod_{k=1}^{N}\cos\left(\frac{\alpha}{2^k}x\right) = \lim_{N\to\infty}\frac{1}{2^N\pi}\frac{\sin(\alpha x)}{\sin[(\alpha/2^N)x]}. \tag{16}$$

Numerically, Shannon's delta kernel is the most important because of its property of being an element of the Paley–Wiener reproducing kernel Hilbert space $B^2_{1/2}$.

$$f(x) = \int_{-\infty}^{\infty} f(y)\frac{\sin[\pi(x-y)]}{\pi(x-y)}\,\mathrm{d}y \quad \forall f \in B^2_{1/2}, \tag{17}$$

where $\forall f \in B^2_{1/2}$ indicates that, in its Fourier representation, the L^2 function f vanishes outside the interval $[-\frac{1}{2}, \frac{1}{2}]$. The Paley–Wiener reproducing kernel Hilbert space $B^2_{1/2}$ is a subspace of the Hilbert space $L^2(R)$. It is noted that the reproducing kernel Hilbert space is a special class of the Hilbert space. For instance, the space $L^2(R)$ is not a reproducing kernel Hilbert space.

The DSC approximation to the delta distribution is closely related to the theory of wavelets and frames. Mathematically, wavelets are functions generated from a single function by applying dilation and translation. They form building blocks for some spaces, such as $L^2(R)$, whether as a frame or as an orthonormal basis. Such building blocks are computationally important when they have certain regularity and localization in both the time and frequency domains. Physically, the wavelet transform is a mathematical technique that can be used to split a signal into different frequency bands or components so that each component can be studied with a resolution matched to its scale, thus providing excellent frequency and spatial resolution, and achieving computational efficiency.

Shannon's wavelet is one of the most important examples and its scaling function is Shannon's delta kernel,

$$\phi(x) = \frac{\sin(\pi x)}{\pi x}. \tag{18}$$

As a delta kernel, it is normalized

$$\hat{\phi}(0) = \int \phi(x)\,\mathrm{d}x = 1, \tag{19}$$

and its Fourier transform is given by the characteristic function $\hat{\phi}(\omega) = \chi_{[-1/2,1/2]}$. It is easy to see that

$$\sum_{n=-\infty}^{\infty} \hat{\phi}(\omega + n) = 1 \tag{20}$$

and

$$\sum_{n=-\infty}^{\infty} |\hat{\phi}(\omega + n)|^2 = 1. \tag{21}$$

Equation (21) is a consequence of orthonormality. In fact, the sequence of functions $\{\phi(x-n)\}_{n=-\infty}^{\infty}$ is orthonormal.

Shannon's mother wavelet can be constructed from Shannon's delta kernel (Shannon's wavelet scaling function)

$$\psi(x) = \frac{\sin(2\pi x) - \sin(\pi x)}{\pi x} \tag{22}$$

with its Fourier expression

$$\hat{\psi}(\omega) = \chi_{[-1,1]}(\omega) - \chi_{[-1/2,1/2]}(\omega). \tag{23}$$

This is recognized as the ideal band pass filter and it satisfies the orthonormality conditions

$$\sum_{n=-\infty}^{\infty} \hat{\psi}(\omega + n) = 1 \tag{24}$$

and

$$\sum_{n=-\infty}^{\infty} |\hat{\psi}(\omega + n)|^2 = 1. \tag{25}$$

Technically, it can be shown that a system of orthogonal wavelets is generated from a single function, a "mother" wavelet ψ, by standard operations of translation and dilation

$$\psi_{mn}(x) = 2^{-m/2}\psi\left(\frac{x}{2^m} - n\right), \quad m, n \in Z. \tag{26}$$

A family of Shannon's wavelet scaling functions $\{\psi_{mn}(x)\}_{n,m\in Z}$ span a series of orthogonal wavelet subspaces $\{W_m\}_{m\in Z}$ satisfying

$$\bigoplus_{m\in Z} W_m = L^2(R). \tag{27}$$

Alternatively, a family of Shannon's wavelet scaling functions $\{\phi_{mn}(x)\}_{n.m\in Z}$ are constructed from a single Shannon's delta kernel

$$\phi_{mn}(x) = 2^{-m/2}\phi\left(\frac{x}{2^m} - n\right), \quad m, n \in Z. \tag{28}$$

They span a series of nested wavelet subspaces $\{V_m\}_{m\in Z}$, each corresponds to a different resolution

$$\cdots \subset V_{-1} \subset V_0 \subset V_1 \subset \cdots \subset L^2(R). \tag{29}$$

This nested structure provides the conceptual basis for the wavelet multi-resolution analysis.

From the point of view of signal processing, Shannon's delta kernel ϕ_α corresponds to a family of *ideal low-pass filters*, each with a different bandwidth

$$\phi_\alpha(x) = \frac{\sin(\alpha x)}{\pi x}. \tag{30}$$

Their corresponding wavelet expression,

$$\psi_\alpha(x) = \frac{\sin(2\alpha\pi) - \sin(\alpha x)}{\pi x} \tag{31}$$

and band pass filters. However, Shannon's wavelet system is seldom used in real applications because it requires infinitely many data points. In the next subsection, we discuss a practical approach for generating powerful filters from Shannon's delta kernel.

2.2. REGULARIZATION

Both $\phi(x)$ and its associated wavelet play a crucial role in information theory and the theory of signal processing. However, their usefulness is limited by the fact that $\phi(x)$ and $\psi(x)$ are infinite impulse response (IIR) filters and their Fourier transforms $\hat{\phi}(\omega)$ and $\hat{\psi}(\omega)$

are not differentiable. From the computational point of view, $\phi(x)$ and $\psi(x)$ do not have finite moments in the co-ordinate space; in other words, they are delocalized. The non-local feature in co-ordinates is related to its bandlimited character in the Fourier representation by the Heisenberg uncertainty principle. To improve the smoothness and regularity of Shannon's low pass filter, we can apply a regularization procedure:

$$\tilde{\Phi}_\sigma(x) = R_\sigma(x)\phi(x), \quad (\sigma > 0), \tag{32}$$

where R_σ is a *regularizer* which has properties

$$\lim_{\sigma \to \infty} R_\sigma(x) = 1 \tag{33}$$

and

$$R_\sigma(0) = 1. \tag{34}$$

Here equation (33) is a general condition that a regularizer must satisfy, while equation (34) is specifically for a *delta regularizer*, which is used in regularizing a delta kernel. Various delta regularizers can be used for numerical computations. An excellent one is the Gaussian

$$R_\sigma(x) = \exp\left[-\frac{x^2}{2\sigma^2} \right]. \tag{35}$$

An immediate benefit of the regularized Shannon's kernel function equation (32) is that its Fourier transform is infinitely differentiable because the Gaussian is an element of the Schwarz class functions. Qualitatively, all kernels of the Dirichlet type oscillate in the co-ordinate representation. Shannon's kernel has a long tail which is proportional to $\frac{1}{x}$, whereas the regularized kernels decay exponentially fast, especially when the σ is very small. In the Fourier representation, Shannon's kernel is an ideal low-pass filter, which is discontinuous at $\omega = \frac{1}{2}$. In contrast, all regularized Shannon's kernels have an "optimal" shape in their frequency responses. Of course, they all reduce to Shannon's low pass filter at the limit.

$$\lim_{\sigma \to \infty} \Phi_\sigma(x) = \lim_{\sigma \to \infty} \frac{\sin(\pi x)}{\pi x} \mathrm{e}^{-x^2/(2\sigma^2)} = \frac{\sin(\pi x)}{\pi x}. \tag{36}$$

Quantitatively, one can examine the normalization of $\Phi_\sigma(x)$

$$\hat{\Phi}_\sigma(0) = \int \Phi_\sigma(x)\,\mathrm{d}x = \sqrt{2\pi}\sigma \sum_{k=0}^{\infty} \frac{(-1)^k}{k!(2k+1)} \left(\frac{\pi\sigma}{\sqrt{2}} \right)^{2k}. \tag{37}$$

By means of the error function, $\mathrm{erf}(z) = (2/\sqrt{\pi}) \int_0^z \mathrm{e}^{-t^2}\,\mathrm{d}t$, equation (37) can be rewritten as

$$\begin{aligned} \hat{\Phi}_\sigma(0) = \mathrm{erf}\left(\frac{\pi\sigma}{\sqrt{2}} \right) &= 1 - \sqrt{\frac{2}{\pi}} \frac{1}{\sigma} \mathrm{e}^{-\sigma^2 x^2/2} \int_0^\infty \mathrm{e}^{-[t^2/2\sigma^2)] - \pi t}\,\mathrm{d}t \\ &= 1 - \mathrm{erfc}\left(\frac{\pi\sigma}{\sqrt{2}} \right), \end{aligned} \tag{38}$$

where erfc(z) is the complementary error function. Note that for a given $\sigma > 0$, erfc $(\pi\sigma/\sqrt{2})$ is positive definite. Thus, $\hat{\Phi}_\sigma(0)$ is always less than unity except at a limit of $\sigma \to \infty$.

In fact, $\Phi_\sigma(x)$ does not really satisfy the requirement, as given by equation (19), for a wavelet scaling function. However, when we choose $\sigma \gg \sqrt{2}/\pi$, which is the case in many practical applications, the residue term, erfc$(\pi\sigma/\sqrt{2})$, approaches zero very quickly. As a result, $\hat{\Phi}_\sigma(0)$ is extremely close to unity. Therefore, we call the regularized Shannon's delta kernel Φ_σ a quasi-wavelet scaling function.

It can be expected that a (quasi) wavelet generated by the difference of two regularized Shannon's delta kernels

$$\psi_\sigma(x) = \frac{\sin(2\pi x)}{\pi x} e^{-2x^2/\sigma^2} - \frac{\sin(\pi x)}{\pi x} e^{-x^2/(2\sigma^2)} \tag{39}$$

will also have excellent smooth and decay properties in both co-ordinate and Fourier representations.

2.3. DISCRETIZATION

For the purpose of digital computations, it is necessary to discretize various delta kernels. To this end, we should examine a *sampling basis* given by Shannon's delta kernel

$$S_k(x) = K(x, x_k) = \frac{\sin[\pi(x - x_k)]}{\pi(x - x_k)}, \quad x_k = k \quad \forall k \in Z, \tag{40}$$

where the symbol Z denotes the set of all integers. This sampling basis is an element of the Paley–Wiener reproducing kernel Hilbert space. Hence, it provides a *discrete representation* of every (continuous) function in $B^2_{1/2}$, that is

$$f(x) = \sum_{k \in Z} f(x_k) S_k(x). \tag{41}$$

This is recognized as Shannon's sampling theorem and it means that one can recover a continuous bandlimited L^2 function from a set of discrete values. Equation (41) is particularly important to information theory and the theory of sampling because it satisfies the interpolation condition

$$S_n(x_m) = \delta_{n,m}, \tag{42}$$

where $\delta_{m,k}$ is the Kronecker delta function. Note that Shannon's delta kernel is obviously interpolative on Z. Computationally, being interpolative is of particular importance for numerical accuracy and simplicity.

On a grid of arbitrary spacing Δ, Shannon's sampling theorem can be modified as

$$f(x) = \sum_{k \in Z} f(x_k) \frac{\sin[(\pi/\Delta)(x - x_k)]}{(\pi/\Delta)(x - x_k)}. \tag{43}$$

This suggests that we can discretize the regularized Shannon's delta kernel as

$$\Phi_{\sigma,\Delta}(x - x_k) = \frac{\sin[(\pi/\Delta)(x - x_k)]}{(\pi/\Delta)(x - x_k)} e^{-(x - x_k)^2/(2\sigma^2)}. \tag{44}$$

It is noted that if Δ is chosen as the spatial mesh size (this is, in general, not required in signal and image processing), $\Phi_{\sigma,\Delta}(x - x_k)$ retains the interpolation property,

$$\Phi_{\sigma,\Delta}(x_m - x_k) = \delta_{m,k}. \tag{45}$$

This is of particular merit for numerical computations.

In practical applications, equation (43) can never be realized because it requires infinitely many sampling data. Therefore, it is both necessary and convenient to truncate the infinite summation in equation (43) to a finite $(2M + 1)$ summation

$$f(x) \approx \sum_{k=-M}^{M} \delta_{\sigma,\Delta}(x - x_k) f(x_k), \tag{46}$$

where $\delta_{\sigma,\Delta}(x - x_k)$ is a collective symbol for any (regularized) delta kernels. The truncation error is dramatically reduced by the introduction of the delta regularizer. A proof of this is given by Qian and Wei [38]. They have provided a mathematical estimation for the choice of M, σ and Δ. For example, if the L^2 error for approximating an L^2 function f is set to $10^{-\eta}$, the following relations are to be satisfied:

$$r(\pi - B\Delta) > \sqrt{4{\cdot}61\eta} \quad \text{and} \quad \frac{M}{r} > \sqrt{4{\cdot}61\eta}, \tag{47}$$

where $r = \sigma/\Delta$ and B is the frequency bound for the function of interest, f. The first inequality states that for a given grid size Δ, a large r is required for approximating high-frequency component of an L^2 function. The second inequality indicates that if one chooses the ratio $r = 3$, then the half-bandwidth $M \sim 30$ can be used to ensure the highest accuracy in a double precision computation ($\eta = 15$). Certainly, such accuracy might not be necessary for many engineering computations. Even in such cases, due to its feature of controllable accuracy, the DSC algorithm can be very efficient in delivering a given accuracy with fewer grid points.

In a way similar to the discretization of equation (44), we use the following regularized discrete expression for the Dirichlet kernel:

$$\frac{\sin[(l + \frac{1}{2})(x - x')]}{2\pi \sin[\frac{1}{2}(x - x')]} \to \frac{\sin[(\pi/\Delta)(x - x_k)]}{(2L + 1)\sin[(\pi/\Delta)(x - x_k)/(2L + 1)]} \exp\left[-\frac{(x - x_k)^2}{2\sigma^2} \right]. \tag{48}$$

Like the regularized Shannon's kernel filter, the present regularized Dirichlet kernel filter has rapid decay property. In comparison with Shannon's kernel, the Dirichlet kernel has one more parameter L which can be optimized to achieve better results in computations. Usually, we set a sufficiently large L for various numerical applications. A regularized discrete expression for the modified Dirichlet kernel is

$$\frac{\sin[(l + \frac{1}{2})(x - x')]}{2\pi \tan[\frac{1}{2}(x - x')]} \to \frac{\sin[(\pi/\Delta)(x - x_k)]}{(2L + 1)\tan[(\pi/\Delta)(x - x_k)/(2L + 1)]} \exp\left[-\frac{(x - x_k)^2}{2\sigma^2} \right]. \tag{49}$$

Obviously, the regularized Dirichlet kernel reduces to the regularized Shannon's delta kernel when L is sufficiently large

$$\lim_{L \to \infty} \frac{\sin[(\pi/\Delta)(x - x_k)]}{(2L + 1)\sin[(\pi/\Delta)(x - x_k)/(2L + 1)]} \exp\left[-\frac{(x - x_k)^2}{2\sigma^2} \right]$$

$$= \lim_{L \to \infty} \frac{\sin[(\pi/\Delta)(x - x_k)]}{(2L+1)\tan[(\pi/\Delta)(x - x_k)/(2L+1)]} \exp\left[-\frac{(x - x_k)^2}{2\sigma^2} \right]$$

$$= \frac{\sin[(\pi/\Delta)(x - x_k)]}{(\pi/\Delta)(x - x_k)} \mathrm{e}^{-(x - x_k)^2/(2\sigma^2)}. \tag{50}$$

Finally, a similar de la Vallée Poussin kernel filter is given by

$$\frac{1}{\pi\alpha} \frac{\cos[\alpha(x - x')] - \cos[2\alpha(x - x')]}{(x - x')^2}$$

$$\to \frac{2}{3} \frac{\cos[(\pi/\bar{\Delta})(x - x_k)] - \cos[(2\pi/\bar{\Delta})(x - x_k)]}{[(\pi/\bar{\Delta})(x - x_k)]^2} \exp\left[-\frac{(x - x_k)^2}{2\sigma^2} \right], \tag{51}$$

where $\bar{\Delta} = \frac{3}{2}\Delta$. Since π/Δ is proportional to the highest frequency which can be reached in the Fourier representation, the Δ should be very small for a given problem involving very oscillatory functions or very high frequency components.

2.4. APPROXIMATION OF DERIVATIVES

For the solution of differential equations, approximation to derivatives are required. Such approximation can be constructed by using DSC kernels of the delta type with $n \neq 0$. Let us consider a one-dimensional, nth order DSC kernel of the delta type

$$\delta^{(n)}_{\sigma,\Delta}(x - x_k), \quad (n = 0, 1, 2, \dots). \tag{52}$$

Here $\delta^{(0)}_{\sigma,\Delta}(x - x_k) = \delta_{\sigma,\Delta}(x - x_k)$ is the DSC delta kernel described in equation (46). The higher order derivative terms $\delta^{(n)}_{\sigma,\Delta}(x_m - x_k)$ are given by differentiation

$$\delta^{(n)}_{\sigma,\Delta}(x_m - x_k) = \left[\left(\frac{\mathrm{d}}{\mathrm{d}x} \right)^n \delta_{\sigma,\Delta}(x - x_k) \right]_{x = x_m}. \tag{53}$$

These derivatives can be regarded as high pass filters. The filters corresponding to the derivatives of Shannon's kernel decay slowly as x increases, whereas the regularized filters are Schwarz class functions and have controlled residual amplitudes at large x values. In the Fourier representation, the derivatives of Shannon's kernel are discontinuous at certain points. In contrast, the derivatives of regularized kernels are all continuous and can be made very close to those of Shannon's, if desired.

The differentiation in equation (53) can be *analytically* carried out for a given $\delta_{\sigma,\Delta}(x - x_k)$. For example, if

$$\delta_{\sigma,\Delta}(x - x_k) = \frac{\sin[(\pi/\Delta)(x - x_k)]}{(\pi/\Delta)(x - x_k)} \mathrm{e}^{-(x - x_k)^2/(2\sigma^2)}, \text{ we have for } x \neq x_k$$

$$\delta^{(1)}_{\sigma,\Delta}(x - x_k) = \frac{\cos[(\pi/\Delta)(x - x_k)]}{(x - x_k)} \exp\left(-\frac{(x - x_k)^2}{2\sigma^2} \right)$$

$$- \frac{\sin[(\pi/\Delta)(x - x_k)]}{(\pi/\Delta)(x - x_k)^2} \exp\left(-\frac{(x - x_k)^2}{2\sigma^2} \right)$$

$$- \frac{\sin[(\pi/\Delta)(x - x_k)]}{(\pi/\Delta)\sigma^2} \exp\left(-\frac{(x - x_k)^2}{2\sigma^2} \right), \tag{54}$$

$$\delta^{(2)}_{\sigma,\Delta}(x-x_k) = -\frac{(\pi/\Delta)\sin[(\pi/\Delta)(x-x_k)]}{(x-x_k)}\exp\left(-\frac{(x-x_k)^2}{2\sigma^2}\right)$$
$$-2\frac{\cos[(\pi/\Delta)(x-x_k)]}{(x-x_k)^2}\exp\left(-\frac{(x-x_k)^2}{2\sigma^2}\right)$$
$$-2\frac{\cos[(\pi/\Delta)(x-x_k)]}{\sigma^2}\exp\left(-\frac{(x-x_k)^2}{2\sigma^2}\right)$$
$$+2\frac{\sin[(\pi/\Delta)(x-x_k)]}{(\pi/\Delta)(x-x_k)^3}\exp\left(-\frac{(x-x_k)^2}{2\sigma^2}\right)$$
$$+\frac{\sin[(\pi/\Delta)(x-x_k)]}{(\pi/\Delta)(x-x_k)\sigma^2}\exp\left(-\frac{(x-x_k)^2}{2\sigma^2}\right)$$
$$+\frac{\sin[(\pi/\Delta)(x-x_k)]}{(\pi/\Delta)\sigma^4}(x-x_k)\exp\left(-\frac{(x-x_k)^2}{2\sigma^2}\right), \tag{55}$$

$$\delta^{(3)}_{\sigma,\Delta}(x-x_k) = -\frac{(\pi^2/\Delta^2)\cos[(\pi/\Delta)(x-x_k)]}{(x-x_k)}\exp\left(-\frac{(x-x_k)^2}{2\sigma^2}\right)$$
$$+3\frac{(\pi/\Delta)\sin[(\pi/\Delta)(x-x_k)]}{(x-x_k)^2}\exp\left(-\frac{(x-x_k)^2}{2\sigma^2}\right)$$
$$+3\frac{(\pi/\Delta)\sin[(\pi/\Delta)(x-x_k)]}{\sigma^2}\exp\left(-\frac{(x-x_k)^2}{2\sigma^2}\right)$$
$$+6\frac{\cos[(\pi/\Delta)(x-x_k)]}{(x-x_k)^3}\exp\left(-\frac{(x-x_k)^2}{2\sigma^2}\right)$$
$$+3\frac{\cos[(\pi/\Delta)(x-x_k)]}{(x-x_k)\sigma^2}\exp\left(-\frac{(x-x_k)^2}{2\sigma^2}\right)$$
$$+3\frac{(x-x_k)\cos[(\pi/\Delta)(x-x_k)]}{\sigma^4}\exp\left(-\frac{(x-x_k)^2}{2\sigma^2}\right)$$
$$-6\frac{\sin[(\pi/\Delta)(x-x_k)]}{(\pi/\Delta)(x-x_k)^4}\exp\left(-\frac{(x-x_k)^2}{2\sigma^2}\right)$$
$$-3\frac{\sin[(\pi/\Delta)(x-x_k)]}{(\pi/\Delta)(x-x_k)^2\sigma^2}\exp\left(-\frac{(x-x_k)^2}{2\sigma^2}\right)$$
$$-\frac{(x-x_k)^2\sin[(\pi/\Delta)(x-x_k)]}{(\pi/\Delta)\sigma^6}\exp\left(-\frac{(x-x_k)^2}{2\sigma^2}\right), \tag{56}$$

and

$$\begin{aligned}\delta^{(4)}_{\sigma,\Delta}(x-x_k) = {} & 4\frac{(\pi^2/\Delta^2)\cos[(\pi/\Delta)(x-x_k)]}{(x-x_k)^2}\exp\left(-\frac{(x-x_k)^2}{2\sigma^2}\right)\\ & + \frac{(\pi^3/\Delta^3)\sin[(\pi/\Delta)(x-x_k)]}{(x-x_k)}\exp\left(-\frac{(x-x_k)^2}{2\sigma^2}\right)\\ & + 4\frac{(\pi^2/\Delta^2)\cos[(\pi/\Delta)(x-x_k)]}{\sigma^2}\exp\left(-\frac{(x-x_k)^2}{2\sigma^2}\right)\\ & - 12\frac{(\pi/\Delta)\sin[(\pi/\Delta)(x-x_k)]}{(x-x_k)^3}\exp\left(-\frac{(x-x_k)^2}{2\sigma^2}\right)\\ & - 6\frac{(\pi/\Delta)\sin[(\pi/\Delta)(x-x_k)]}{(x-x_k)\sigma^2}\exp\left(-\frac{(x-x_k)^2}{2\sigma^2}\right)\\ & - 6\frac{(\pi/\Delta)(x-x_k)\sin[(\pi/\Delta)(x-x_k)]}{\sigma^4}\exp\left(-\frac{(x-x_k)^2}{2\sigma^2}\right)\\ & - 24\frac{\cos[(\pi/\Delta)(x-x_k)]}{(x-x_k)^4}\exp\left(-\frac{(x-x_k)^2}{2\sigma^2}\right)\\ & - 12\frac{\cos[(\pi/\Delta)(x-x_k)]}{(x-x_k)^2\sigma^2}\exp\left(-\frac{(x-x_k)^2}{2\sigma^2}\right)\\ & - 4\frac{(x-x_k)^2\cos[(\pi/\Delta)(x-x_k)]}{\sigma^6}\exp\left(-\frac{(x-x_k)^2}{2\sigma^2}\right)\\ & + 24\frac{\sin[(\pi/\Delta)(x-x_k)]}{(\pi/\Delta)(x-x_k)^5}\exp\left(-\frac{(x-x_k)^2}{2\sigma^2}\right)\\ & + 12\frac{\sin[(\pi/\Delta)(x-x_k)]}{(\pi/\Delta)(x-x_k)^3\sigma^2}\exp\left(-\frac{(x-x_k)^2}{2\sigma^2}\right)\\ & + 3\frac{\sin[(\pi/\Delta)(x-x_k)]}{(\pi/\Delta)(x-x_k)\sigma^4}\exp\left(-\frac{(x-x_k)^2}{2\sigma^2}\right)\\ & - 2\frac{(x-x_k)\sin[(\pi/\Delta)(x-x_k)]}{(\pi/\Delta)\sigma^6}\exp\left(-\frac{(x-x_k)^2}{2\sigma^2}\right)\\ & + \frac{(x-x_k)^3\sin[(\pi/\Delta)(x-x_k)]}{(\pi/\Delta)\sigma^8}\exp\left(-\frac{(x-x_k)^2}{2\sigma^2}\right). \end{aligned} \tag{57}$$

At $x = x_k$, it is convenient to evaluate these derivatives separately

$$\delta^{(1)}_{\sigma,\Delta}(0) = 0, \tag{58}$$

$$\delta^{(2)}_{\sigma,\Delta}(0) = -\frac{1}{3}\frac{3 + (\pi^2/\Delta^2)\sigma^2}{\sigma^2}, \tag{59}$$

$$\delta^{(3)}_{\sigma,\Delta}(0) = 0 \tag{60}$$

and

$$\delta^{(4)}_{\sigma,\Delta}(0) = \frac{1}{5}\frac{15 + 10(\pi^2/\Delta^2)\sigma^2 + (\pi^4/\Delta^4)\sigma^4}{\sigma^4}. \tag{61}$$

Similar expressions for the other DSC kernels described in the last subsection can be easily derived. The performance of a few DSC kernels for fluid dynamic computations and structural analysis was given in reference [35].

Note that the differentiation matrix in equation (53) is generally banded. This has a distinct advantage in large-scale computations.

2.5. TREATMENT OF BOUNDARY CONDITIONS

It is well known that in the continuous case, a derivative at a point exists if and only if both the left derivative and the right derivative exist and are equal. Therefore, with a finite computational domain, a boundary condition involving differentiation, such as the Neumann boundary condition, does not make sense. This is an ill-posed problem from the point of view of mathematics. One way to fix this problem is to extend the domain of definition of the system so that the "boundary condition" is well defined. The basic philosophy behind DSC is that, the original singular convolution has to be recovered from the DSC at a limit of $\Delta x \to 0$. Therefore, at the boundary, a fictitious domain is required to make the boundary condition exactly satisfied at the continuous limit.

In this subsection, the DSC algorithm for treating various boundary conditions is discussed in the context of plate vibration analysis, while the approach can be used for many other applications. We limit our attention to the vibration of rectangular Kirchhoff plates with simply supported, clamped and transversely supported edges. Consider a rectangular plate which has a length l_x, width l_y, thickness h, mass density ρ, modulus of elasticity E, and Poisson's ratio v. The governing differential equation for the plate is given by

$$\frac{\partial^4 w}{\partial x^4} + 2\frac{\partial^4 w}{\partial x^2 \partial y^2} + \frac{\partial^4 w}{\partial y^4} = \frac{\rho h \omega^2}{D} w, \tag{62}$$

where $w(x, y)$ is the transverse displacement of the midsurface of the plate, $D = Eh^3/[12(1 - v^2)]$ the flexural rigidity, and ω the circular frequency. We consider one of the following three types of support conditions for each plate edge:

For simply supported edge (*S*):

$$w = 0, \quad -D\left(\frac{\partial^2 w}{\partial n^2} + v\frac{\partial^4 w}{\partial s^2}\right) = 0. \tag{63}$$

For clamped edge (*C*):

$$w = 0, \quad \frac{\partial w}{\partial n} = 0. \tag{64}$$

For transversely supported edge with non-uniform elastic rotational restraint (E):

$$w = 0, \quad -D\left(\frac{\partial^2 w}{\partial n^2} + v\frac{\partial^2 w}{\partial s^2}\right) = K(s)\frac{\partial w}{\partial n}, \tag{65}$$

where $K(s)$ is the varying elastic rotational stiffness of the plate elastic edge and n and s denote, respectively, the normal and tangential co-ordinates with respect to the rectangular plate edge.

For generality and simplicity, the following dimensionless parameters are introduced:

$$X = \frac{x}{l_x}, \quad Y = \frac{y}{l_y}, \quad W = \frac{w}{l_x}, \quad \lambda = \frac{l_x}{l_y}, \quad \Omega = \omega l_x^2\sqrt{\frac{\rho h}{D}}. \tag{66}$$

Accordingly, we obtain the dimensionless governing equation for the vibration analysis of a rectangular plate as

$$\frac{\partial^4 W}{\partial X^4} + 2\lambda^2\frac{\partial^4 W}{\partial X^2 \partial Y^2} + \lambda^4\frac{\partial^4 W}{\partial Y^4} = \Omega^2 W. \tag{67}$$

Consider a uniform grid having

$$0 = X_0 < X_1 < \cdots < X_N = 1$$

and

$$0 = Y_0 < Y_1 < \cdots < Y_N = 1.$$

To formulate the eigenvalue problem, we introduce a column vector $\mathbf{W}$ as

$$\mathbf{W} = (W_{0,0}, \ldots, W_{0,N}, W_{1,0}, \ldots, W_{N,N})^{\mathrm{T}}$$

with $(N+1)^2$ entries $W_{i,j} = W(X_i, Y_j), (i, j = 0, 1, \ldots, N)$.

Let us define $(N+1)\times(N+1)$ differentiation matrices $\mathbf{D}_q^n (q = X, Y; n = 1, 2, \ldots)$, with their elements given by

$$[\mathbf{D}_q^n]_{i,j} = \delta_{\sigma,\Delta}^{(n)}(q_i - q_j)\,(i, j = 0, \ldots, N), \tag{68}$$

where $\delta_{\sigma,\Delta}^{(n)}(q_i - q_j), (q = X, Y)$ are given by equation (53). Here the matrix is banded to $i - j = -M, \ldots, 0, \ldots, M$. Therefore, the system of linear algebraic equations for the governing equation (67) is given by

$$(\mathbf{D}_X^4 \otimes \mathbf{I} + 2\lambda^2\mathbf{D}_X^2 \otimes \mathbf{D}_Y^2 + \lambda^4\mathbf{I} \otimes \mathbf{D}_Y^4)\mathbf{W} = \Omega^2\mathbf{W}, \tag{69}$$

where $\mathbf{I}$ is the $(N+1)\times(N+1)$ unit matrix and $\otimes$ denotes the tensorial product. Eigenvalues can be evaluated from equation (69) by using a standard solver. However, appropriate boundary conditions are to be implemented before calculating the eigenvalues. This is described below.

We first note that the boundary condition $W = 0$ is easily specified at the boundary. To implement other boundary conditions, we assume, for a function f, the following relation between the inner nodes and the outer nodes on the left boundary:

$$f(X_{-i}) - f(X_0) = a_i[f(X_i) - f(X_0)], \tag{70}$$

where parameters a_i, $(i = 1, \ldots, M)$ are to be decided. After rearrangement, we obtain

$$f(X_{-i}) = a_i f(X_i) + (1 - a_i) f(X_0),\ i = 1, 2, \ldots, M. \tag{71}$$

According to equation (53), we approximate the first and second derivatives by

$$f'(X_0) = \sum_{i=-M}^{M} C_i^1 f(X_i) \tag{72}$$

$$= \left[C_0^1 - \sum_{i=1}^{M} (1 - a_i) C_i^1 \right] f(X_0) + \sum_{i=1}^{M} (1 - a_i) C_i^1 f(X_i) \tag{73}$$

and

$$f''(X_0) = \sum_{i=-M}^{M} C_i^2 f(X_i)$$

$$= \left[C_0^2 + \sum_{i=1}^{M} (1 - a_i) C_i^2 \right] f(X_0) + \sum_{i=1}^{M} (1 + a_i) C_i^2 f(X_i),$$

respectively, and C_i^1 and C_i^2 correspond to $\delta_{\sigma,\Delta}^{(1)}(X_i - X_0)$ and $\delta_{\sigma,\Delta}^{(2)}(X_i - X_0)$ respectively.

For simply supported edges, the boundary conditions reduce to

$$f(X_0) = 0, f''(X_0) = 0. \tag{74}$$

These are satisfied by choosing $a_i = -1, i = 1, 2, \ldots, M$. This is the so-called *anti-symmetric extension* [27].

For clamped edges, i.e., the boundary conditions require

$$f(X_0) = 0, f'(X_0) = 0. \tag{75}$$

These are satisfied by choosing $a_i = 1, i = 1, 2, \ldots, M$. This is the *symmetric extension* [27].

For a transversely supported edge, the boundary conditions are

$$f(X_0) = 0, f''(X_0) - K f'(X_0) = 0. \tag{76}$$

Hence, the equation is given by

$$\sum_{i=1}^{M} (1 + a_i) C_i^2 f(X_i) - K \sum_{i=1}^{M} (1 - a_i) C_i^1 f(X_i) = 0. \tag{77}$$

Further simplification of the above equation gives

$$\sum_{i=1}^{M} [(1 + a_i) C_i^2 - K(1 - a_i) C_i^1] f(X_i) = 0. \tag{78}$$

One way to satisfy equation (78) is to choose

$$a_i = \frac{K C_i^1 - C_i^2}{K C_i^1 + C_i^2}, \quad i = 1, 2, \ldots, M. \tag{79}$$

Expressions for the right boundary can be derived in a similar way.

For the continuous non-uniform (elastic) boundary conditions, the rotational spring coefficients $K_1(Y)$, $K_2(Y)$, $K_3(X)$ and $K_4(X)$ are taken as

$$K_1(Y) = K_2(Y) = K'Y(1 - Y), \tag{80}$$

$$K_3(X) = K_4(X) = K'X(1 - X)/\lambda, \tag{81}$$

where K' is the non-dimensional spring coefficient, $K' = K_0 l_x^3/D$. Obviously, the implementation of these rotational spring coefficients leads to a minor modification of the matrix in equation (69).

In general, the matrix given by equation (69) is very sparse, particularly when N is much larger than M. However, due to the implementation of boundary conditions, the matrix is neither symmetric nor banded.

3. RESULTS AND DISCUSSION

In this section, we explore the usefulness and test the accuracy of the DSC algorithm for the study of the vibration of rectangular plates with simply supported, clamped and transversely supported with non-uniform elastic rotational restraint edges. We consider all possible combinations of the three boundary conditions, which give rise to 21 distinct configurations as depicted in Figure 1.

These 21 cases can be classified into three types. Type 1 has three cases that are confined by either simply supported, or clamped, or transversely supported with non-uniform elastic rotational restraint edges. Type 2 has 12 distinct configurations that involve two different boundary conditions. The last type consists of six non-trivial cases that involve all of the three boundary conditions. The rest of this section is devoted to convergence and comparison studies. All DSC results are obtained by using a standard eigenvalue solver.

3.1. CONVERGENCE STUDY

We choose one configuration from each type for the convergence study (Cases 1, 13 and 21). Case 1 (all sides simply supported: S–S–S–S) is used for the first test. This problem has analytical solution and has been used by many authors to test their methods [17, 21, 18, 22, 25, 23]. In earlier studies [35, 31], the DSC algorithm was utilized to compute vibration modes. The results were accurate to at least 11 significant figures for the first 100 eigenvalues by using 33 grid points in each dimension. In the present study, we test the rate of convergence for the first 8 eigenvalues. To test the proposed algorithm, a variety of DSC kernel parameters are studied. We choose $N = M$ in the convergence study with the M values varying from 16, 20, 24, 28, to 32, and their corresponding σ/Δ values being chosen as 2·5, 2·6, 2·8, 3·2 and 3·6 respectively.

Table 1 presents the convergence test of Case 1. It can be seen that the results obtained by using DSC have reached complete convergence for 26 grid points in each dimension. To our knowledge, the present DSC results are the most accurate, so far reported for this case. However, such a high accuracy might not be necessary for ordinary engineering computations and designs. Nevertheless, the reliability implied by the accuracy has far-reaching ramifications. Moreover, the present results provide confidence to use the DSC algorithm for more general problems in plate analysis. A comparison of eigenvalues obtained by various computational methods is given in the next subsection.

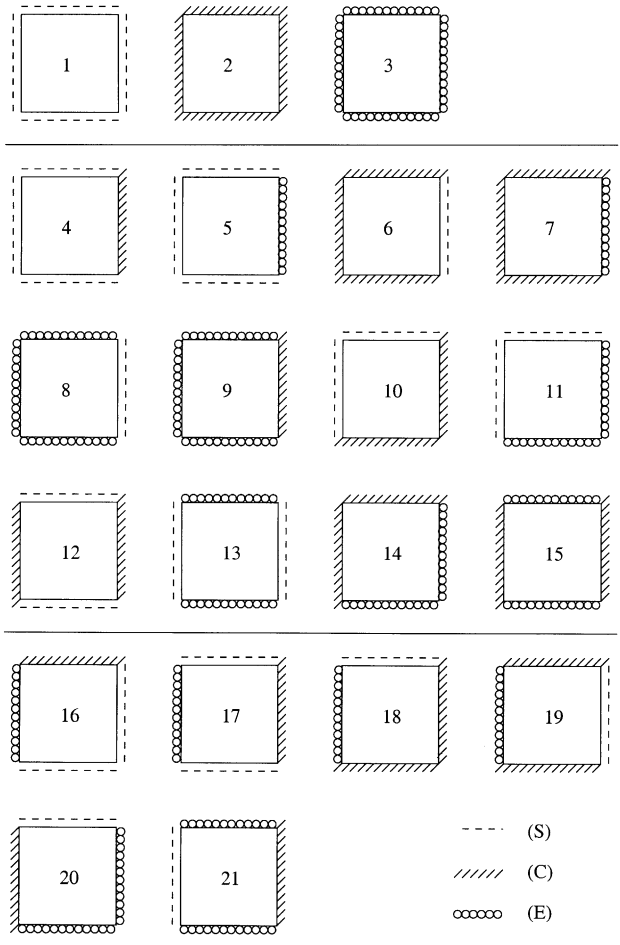

Figure 1. Twenty-one distinct cases according to different combinations of S, C and E edges.

Further, Case 13 (E–S–E–S) is considered for the numerical test of convergence. This problem has also been studied by other researchers [19, 24, 26]. Therefore, a comparison can be made with the existing literature and is given in the next subsection. The DSC results are obtained by using a variety of grid points, which are presented in Table 2.

It is found that the rate of convergence is slightly lower than that in Case 1 because the boundary conditions are more complicated. However, the convergence is fully "satisfactory" by the general standard in the literature. In general, for a discrete representation, the non-uniform boundary condition, which is a continuous function, is not unique, i.e., the boundary condition changes as the number of grid points changes. As a consequence, the numerical solution cannot be unique except at the continuous limit. Therefore, slow convergence with the non-uniform boundary condition will appear in all methods that take discrete point approximations. However, this may not be a problem in a class of other methods which do not use point approximation, e.g., the Ritz method. However, the Ritz method ususally does not explicitly handle all the boundary conditions in the analysis of plates.

The third test problem is (randomly) chosen as Case 21 (S–E–C–E). This problem contains a combination of the three different boundary conditions. The DSC results are

TABLE 1

Convergence study of frequency parameters for S–S–S–S (Case 1) square plate

N	Ω_1	Ω_2	Ω_3	Ω_4
26	19·739209	49·3480220	49·3480220	78·9568352
27	19·739209	49·3480220	49·3480220	78·9568352
28	19·739209	49·3480220	49·3480220	78·9568352
29	19·739209	49·3480220	49·3480220	78·9568352
30	19·739209	49·3480220	49·3480220	78·9568352
31	19·739209	49·3480220	49·3480220	78·9568352
32	19·739209	49·3480220	49·3480220	78·9568352
N	Ω_5	Ω_6	Ω_7	Ω_8
26	98·6960440	98·6960440	128·3048572	128·3048572
27	98·6960440	98·6960440	128·3048572	128·3048572
28	98·6960440	98·6960440	128·3048572	128·3048572
29	98·6960440	98·6960440	128·3048572	128·3048572
30	98·6960440	98·6960440	128·3048572	128·3048572
31	98·6960440	98·6960440	128·3048572	128·3048572
32	98·6960440	98·6960440	128·3048572	128·3048572

TABLE 2

Convergence study of frequency parameters for S–E–S–E (Case 13) square plate with $K' = 1$

N	Ω_1	Ω_2	Ω_3	Ω_4	Ω_5	Ω_6	Ω_7	Ω_8
26	19·986	49·431	49·749	79·167	98·735	99·158	128·431	128·600
27	19·985	49·431	49·748	79·166	98·735	99·157	128·430	128·599
28	19·985	49·431	49·748	79·166	98·735	99·156	128·430	128·599
29	19·985	49·431	49·748	79·166	98·735	99·155	128·430	128·598
30	19·985	49·431	49·747	79·165	98·735	99·155	128·430	128·598
31	19·985	49·431	49·747	79·165	98·735	99·154	128·429	128·597
32	19·985	49·431	49·747	79·165	98·735	99·153	128·429	128·597

TABLE 3

Convergence study of frequency parameters for E–C–E–S (Case 21) square plate with $K' = 1$

N	Ω_1	Ω_2	Ω_3	Ω_4	Ω_5	Ω_6	Ω_7	Ω_8
26	23·855	52·063	58·724	86·342	100·731	113·279	134·096	140·985
27	23·855	52·063	58·723	86·341	100·730	113·277	134·094	140·982
28	23·855	52·062	58·723	86·340	100·729	113·276	134·092	140·980
29	23·855	52·062	58·722	86·339	100·728	113·275	134·091	140·978
30	23·855	52·062	58·722	86·338	100·727	113·274	134·089	140·976
31	23·855	52·061	58·722	86·338	100·726	113·273	134·088	140·975
32	23·855	52·061	58·721	86·337	100·725	113·272	134·087	140·974

given in Table 3. It can be noted that in this case, the rate of convergence is about the same as that for Case 13. Nevertheless, the present rate of convergence is still very fast and the results are highly reliable for ordinary engineering analysis and design.

3.2. COMPARISON STUDY

To further validate the present approach, we study the effect of spring coefficients on the fundamental frequency. The number of the grid point is chosen as $N = 32$ and based on the

TABLE 4

Comparison study of fundamental frequency parameters of rectangular plates with non-uniform boundary conditions

		S–E–S–E				C–E–C–E			
λ	K'	a	b	c	DSC	a	b	c	DSC
0·5	0	12·337	12·34	12·337	12·337	23·814	23·82	23·816	23·816
	0·1	12·334	12·34	12·341	12·340	23·844	23·82	23·818	23·819
	1	12·372	12·38	12·379	12·362	23·876	23·85	23·839	23·843
	10	12·621	12·66	12·666	12·550	24·136	24·01	23·996	24·019
	100	13·319	13·37	13·364	13·207	24·561	24·41	24·393	24·410
	10^6	13·688	13·70	13·686	13·686	24·566	24·60	24·578	24·579
1	0	19·739	19·74	19·734	19·739	28·951	28·96	28·951	28·952
	0·1	19·757	19·76	19·761	19·764	28·969	28·98	28·966	28·970
	1	19·915	19·95	19·951	19·985	29·219	29·12	29·102	29·128
	10	21·235	21·49	21·487	21·701	32·179	30·24	30·222	30·383
	100	25·799	26·13	26·147	26·356	35·379	33·82	33·796	33·960
	10^6	28·951	28·98	28·951	28·951	35·992	36·01	35·985	35·987

Source: a, reference [19]; b, reference [24]; c, reference [26].

TABLE 5

Frequency parameters (*Type* 1)

Case	λ		Ω_1	Ω_2	Ω_3	Ω_4	Ω_5	Ω_6	Ω_7	Ω_8
1	1	DSC	19·7392	49·3480	49·3480	78·9568	98·6960	98·6960	128·3049	128·3049
		a	19·74	49·35	49·35	78·95	98·69	98·69	128·30	128·30
		b	19·74	49·32	49·34	78·91	98·64	98·68	128·17	128·22
		c	19·7392	49·3480	49·3480	78·9568	98·6960	98·6960	128·3049	128·3049
		d	19·74	49·36	49·38	78·98	98·80	99·21	128·40	128·72
		e	19·7392	49·3495	49·3495	78·9586	98·4154	—	—	—
	$\frac{2}{3}$	DSC	14·2561	27·4156	43·8649	49·3480	57·0244	78·9568	80·0535	93·2129
		c	14·2561	27·4156	43·8649	49·3480	57·0244	78·9568	80·0535	93·2129
	$\frac{3}{2}$	DSC	32·0762	61·6850	98·6960	111·0330	128·3049	177·6529	180·1203	209·7291
		c	32·0762	61·6850	98·6960	111·0330	128·3049	177·6529	180·1203	209·7291
2	1	DSC	35·987	73·402	73·402	108·235	131·604	132·227	165·043	165·043
		c	35·992	73·413	73·413	108·27	131·64	132·24	—	—
		e	35·986	73·399	73·399	108·230	131·418	—	—	—
		f	35·96	73·35	73·35	108·2	131·4	132·2	—	—
	$\frac{2}{3}$	DSC	27·006	41·708	66·131	66·534	79·818	100·84	103·15	125·32
		c	27·010	41·716	66·143	66·552	79·850	100·85	—	—
	$\frac{3}{2}$	DSC	60·764	93·844	148·79	149·70	179·59	226·89	232·09	281·96
		c	60·772	93·860	148·82	149·74	179·66	226·92	—	—
3	1	DSC	20·229	49·829	49·829	79·373	99·140	99·244	128·721	128·721
	$\frac{2}{3}$	DSC	14·820	27·776	44·547	49·646	57·508	79·349	80·327	93·939
	$\frac{3}{2}$	DSC	32·937	62·231	99·731	111·483	129·036	178·245	180·532	210·826

Source: a, reference [17]; b, reference [21]; c, reference [18]; d, reference [22]; e, reference [25]; f, reference [23].

TABLE 6

Frequency parameters (*Type* 2, $\lambda = 1$)

Case		Ω_1	Ω_2	Ω_3	Ω_4	Ω_5	Ω_6	Ω_7	Ω_8
4	DSC	23·6466	51·6750	58·6483	86·1380	100·2711	113·2356	133·7970	140·8563
	a	23·71	52·00	58·65	86·26	100·84	113·22	134·18	140·89
	b	23·62	51·62	58·65	86·16	100·35	113·24	134·00	140·94
	c	23·6463	51·6743	58·6464	86·1345	100·2698	113·2281	133·7910	140·8456
	d	23·65	51·71	58·67	86·17	100·78	113·40	134·22	141·01
5	DSC	19·862	49·389	49·547	79·061	98·715	98·925	128·367	128·451
6	DSC	31·827	63·335	71·083	100·805	116·368	130·372	151·919	159·510
	c	31·829	63·347	71·084	100·83	116·40	130·37	—	—
7	DSC	31·947	63·539	71·124	100·914	116·603	130·392	152·073	159·574
8	DSC	20·106	49·630	49·788	79·269	98·957	99·179	128·575	128·659
9	DSC	24·010	52·114	58·934	86·455	100·750	113·506	134·158	141·129
10	DSC	27·055	60·541	60·789	92·843	114·565	114·713	145·798	146·097
	c	27·056	60·544	60·791	92·865	114·57	114·72	—	—
	e	27·054	60·540	60·788	92·834	114·202	—	—	—
11	DSC	19·984	49·588	49·589	79·165	98·918	98·970	128·513	128·513
12	DSC	28·952	54·745	69·333	94·594	102·220	129·115	140·219	154·803
13	DSC	19·985	49·431	49·747	79·165	98·735	99·153	128·429	128·597
	f	19·951	49·419	49·690	79·134	98·729	—	—	—
	g	19·915	—	—	—	—	—	—	—
	h	19·95	—	—	—	—	—	—	—
14	DSC	27·328	60·818	61·021	93·071	114·841	114·949	146·038	146·303
15	DSC	29·128	55·119	69·397	94·783	102·674	129·148	140·506	154·913
	f	29·102	—	—	—	—	—	—	—
	g	29·219	—	—	—	—	—	—	—
	h	29·12	—	—	—	—	—	—	—

Source: a, reference [17]; b, reference [21]; c, reference [18]; d, reference [22]; e, reference [25]; f, reference [26]; g, reference [19]; h, reference [24].

TABLE 7

Frequency parameters (*Type* 3, $\lambda = 1$)

Case		Ω_1	Ω_2	Ω_3	Ω_4	Ω_5	Ω_6	Ω_7	Ω_8
16	DSC	23·750	51·868	58·685	86·237	100·498	113·254	133·942	140·915
17	DSC	23·803	51·728	58·861	86·256	100·296	113·469	133·868	141·012
18	DSC	27·192	60·654	60·931	92·957	114·643	114·890	145·912	146·207
19	DSC	29·039	54·932	69·365	94·689	102·447	129·131	140·363	154·858
20	DSC	23·906	51·921	58·897	86·355	100·523	113·488	134·013	141·070
21	DSC	23·855	52·061	58·721	86·337	100·725	113·272	134·087	140·974

convergence study, the DSC kernel parameters are chosen as $M = 25$ and $\sigma = 2{\cdot}8\Delta$ in the rest of the calculation (given in Tables 4–7) to ensure that all results are reliable. The DSC results are compared with those obtained by Laura and Gutierrez [24] using the differential quadrature δ-technique, by Leissa *et al.* [19] using the Rayleigh–Ritz and by Shu and Wang using the generalized differential quadrature method [26]. The results of the fundamental frequency are compared in Table 4 for S–E–S–E (Case 13) and C–E–C–E (Case 15) plates, with aspect ratios of 0·5, 1·0 and non-dimensional spring coefficients K' of 0, 0·1, 1·0, 10, 100 and 10^6. The fundamental frequency parameters increase monotonically as the

non-dimensional spring coefficient increases from 0 to 10^6. The present results agree well with those of Leissa *et al.* [19], Laura and Gutierrez [24], and Shu and Wang [26].

Further comparison is made between the DSC results and those in the literature for the three cases in Type 1 with aspect ratios $\lambda = \frac{2}{3}$, 1 and $\frac{3}{2}$. Calculations on Cases 1 and 2 have been reported by many authors [17, 21, 18, 22, 25, 23]. Case 1 is exactly solvable. The more accurate DSC results are listed in Table 1. For Case 2, the results reported by Narita are slightly smaller than those obtained by using the DSC algorithm and other methods. For $\lambda \neq 1$, the DSC results are compared with those given by Leissa [18]. This comparison is listed in Table 5. In the computation for Case 3, i.e., the fully transversely supported plate, spring coefficient K' is taken as 1. In the computation given in Tables 6 and 7, the same value of spring coefficient is used.

Table 6 gives a comparison study of the frequency parameters of Type 2 (Cases 4–15) plates with $\lambda = 1$. Much study can be found in the literature for these cases [17, 21, 18, 22, 25, 26, 19, 24]. We observed that the DSC results agree well with those of others. In particular, the present results are in excellent agreement with those of Leissa [18] obtained by using the Rayleigh approach in Cases 4, 6 and 10.

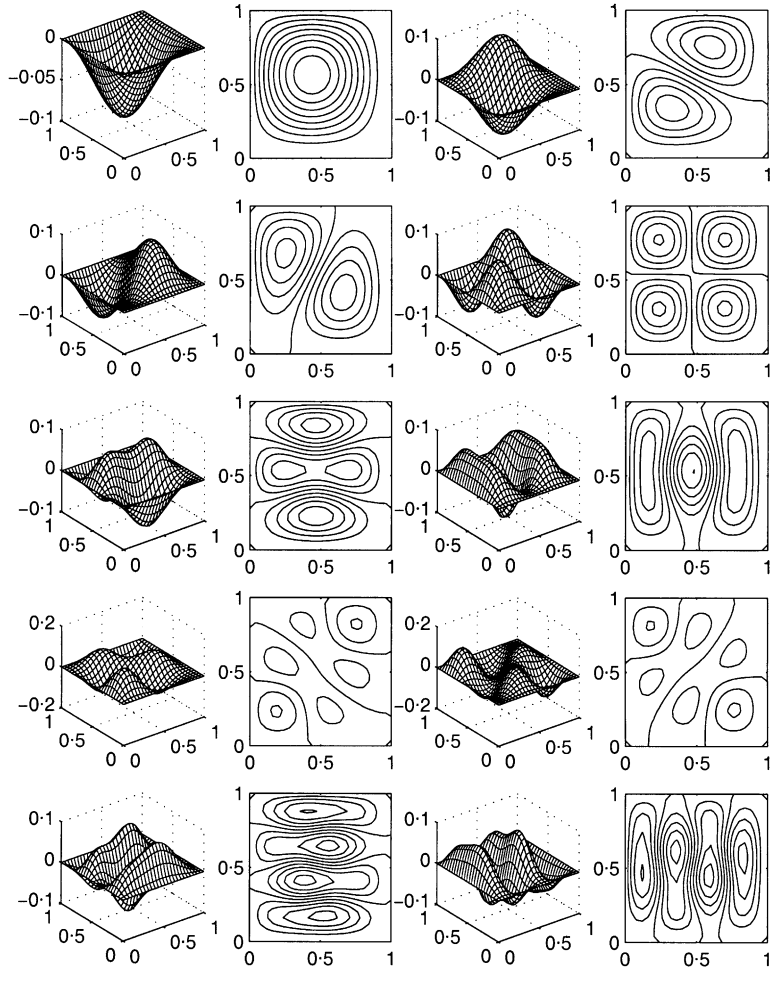

Figure 2. Mesh and contour plots for the first 10 eigenmodes of Case 18.

Frequency parameters for Type 3 cases (Cases 16–21) with $\lambda = 1$ are also listed. It seems to us that these cases have not been reported before. These problems do not have a closed-form solution. Based on convergence tests conducted in the last subsection, it is believed that the DSC results are accurate and reliable. The first ten eigenmodes for Cases 18 and 21 are plotted in Figures 2 and 3 respectively.

It is noted that, for square plates, their corresponding modes 2, 3, 7 and 8 are slightly different. In Case 18, there is an approximate symmetry along one of the two diagonals because the transversely supported (with non-uniform elastic rotational restraint) edge is very close to the simply supported edge when spring coefficient K' is relatively small. Eigenmode patterns similar to that of Case 18 were found in Cases 1, 2, 3, 10, 11 and 14 (for $\lambda = 1$). Patterns in all other cases are similar to that of Case 21.

Rectangular plates with all edges transversely supported with *uniform* elastic rotational restraint were investigated by using the Rayleigh–Ritz method [39], Mukhopadhyay's method [39] and the spline finite strip method [40]. Frequency parameters were reported for the first few eigenmodes. Table 8 lists a comparison study of frequency parameters of the present results and those in the literature. The comparison proceeds with two aspect ratios

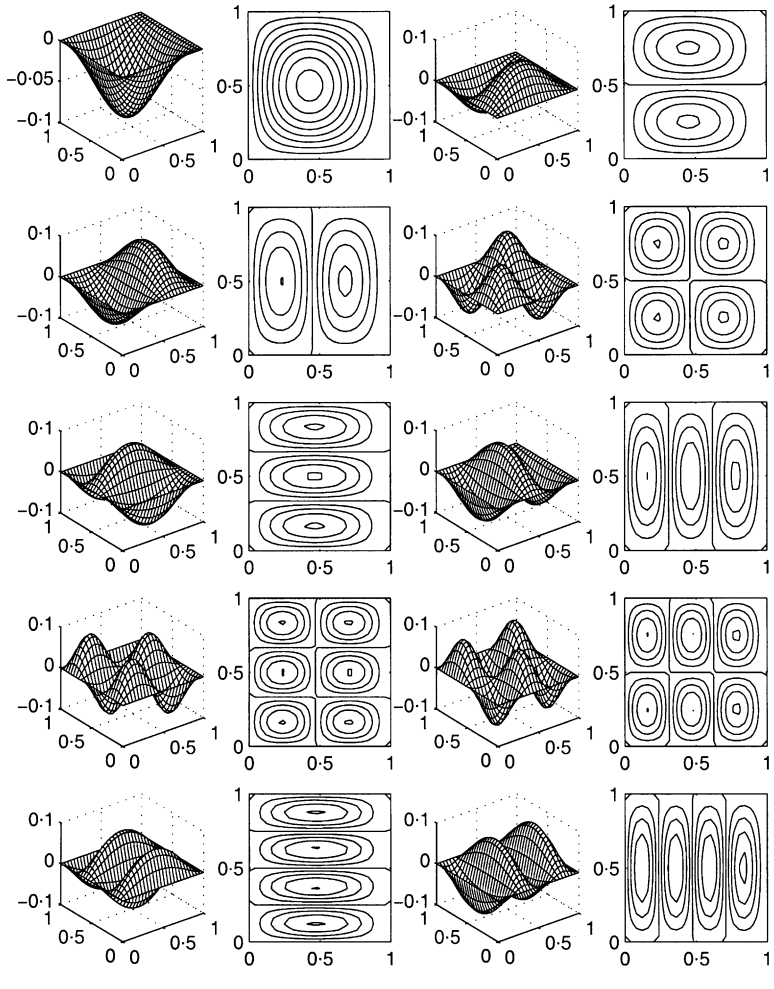

Figure 3. Mesh and contour plots for the first 10 eigenmodes of Case 21.

TABLE 8

Comparison of frequency parameters Ω of rectangular plates with all edges transversely supported with uniform elastic rotational restraint

λ	K		Ω_1	Ω_2	Ω_3	Ω_4	Ω_5	Ω_6	Ω_7	Ω_8
1	0·1	DSC	19·968	49·580	49·580	79·190	98·931	98·931	128·541	128·541
		a	19·937	49·546	49·546	79·155	—	—	—	—
		b	19·936	49·533	49·546	79·142	—	—	—	—
		c	19·937	49·549	49·556	79·164	98·938	99·036	—	—
	1	DSC	21·748	51·474	51·474	81·130	100·900	100·910	130·535	130·535
		a	21·502	51·191	51·191	80·828	—	—	—	—
		b	21·501	51·177	51·191	80·814	—	—	—	—
		c	21·502	51·196	51·202	80·838	100·633	100·736	—	—
	100	DSC	34·758	70·990	79·990	104·804	127·460	128·038	159·995	159·995
		a	34·671	70·781	70·781	104·450	—	—	—	—
		b	34·666	70·746	70·784	104·480	—	—	—	—
		c	34·675	70·801	70·819	104·509	127·236	127·862	—	—
2·5	0·1	DSC	72·815	102·13	151·24	220·18	258·01	287·50	308·01	336·70
		a	72·64	101·99	151·14	220·09	—	—	—	—
		b	72·636	101·99	151·13	220·09	—	—	—	—
		c	72·64	101·99	151·12	220·28	257·88	287·38	—	—
	1	DSC	82·31	109·69	157·13	224·96	269·39	297·99	312·99	346·04
		a	81·03	108·63	156·26	224·21	—	—	—	—
		b	81·03	108·62	156·26	224·20	—	—	—	—
		c	81·04	108·63	156·29	224·40	267·79	296·49	—	—
	100	DSC	142·66	167·97	214·28	282·82	373·22	381·19	407·52	452·69
		a	143·30	167·50	213·50	281·70	—	—	—	—
		b	142·29	167·59	213·68	282·04	—	—	—	—
		c	142·34	167·54	213·69	282·18	372·99	380·38	—	—

Source: a, reference [39] by the Rayleigh–Ritz method; b, reference [39] by Mukhopadhyay's method; c, reference [40] by the spline finite strip method.

($\lambda = 1$ and 2·5) and three rotational spring coefficients ($K = 0{\cdot}1$, 1 and 100). Obviously, DSC results agree quite well with those available in the literature for all eigenmodes.

4. CONCLUSION

This work introduces the discrete singular convolution (DSC) for the treatment of plates with the combinations of simply supported, clamped and transversely supported (with non-uniform elastic rotational restraint) edges. Twenty one non-trivial cases that are constructed from all possible combinations of the three boundary conditions are employed to validate the present approach. A unified scheme is proposed to handle all three boundary conditions. To our knowledge, for the analytically solvable case of all-side simply supported boundary conditions, the DSC results are the most accurate yet available. In all other test problems, the DSC results are consistent with previous ones in the literature. The numerical results confirmed the promising nature of the present approach and the great potential it holds for plate analysis.

ACKNOWLEDGMENT

This work was supported by the National University of Singapore.

REFERENCES

1. C. Lanczos 1938 *Journal of Mathematical Physics* **17**, 123–199. Trigonometric interpolation of empirical and analytical functions.
2. J. W. Cooley and J. W. Tukey 1965 *Mathematics of Computation* **19**, 297–301. An algorithm for the machine calculation of complex Fourier series.
3. B. A. Finlayson and L. E. Scriven 1966 *Applied Mechanics Reviews* **19**, 735–748. The method of weighted residuals—a review.
4. S. A. Orszag 1972 *Studies in Applied Mathematics* **51**, 253–259. Comparison of pseudospectral and spectral approximations.
5. B. Fornberg 1975 *SIAM Journal of Numerical Analysis* **12**, 509–528. On a Fourier method for the integration of hyperbolic equations.
6. G. E. Forsythe and W. R. Wasow 1960 *Finite-Difference Methods for Partial Differential Equations*. New York: Wiley.
7. E. Isaacson and H. B. Keller 1966 *Analysis of Numerical Methods*. New York: Wiley.
8. O. C. Zienkiewicz 1971 *The Finite Element Method in Engineering Science*. London: McGraw-Hill.
9. C. S. Desai and J. F. Abel 1972 *Introduction to the Finite Element Methods*. New York: Van Nostrand Reinhold.
10. J. T. Oden 1972 *The Finite Elements of Nonlinear Continua*. New York: McGraw-Hill.
11. B. Nath 1974 *Fundamentals of Finite Elements for Engineers*. London: Athlone Press.
12. R. T. Fenner 1975 *Finite Element Methods for Engineers*. London: Imperial College Press.
13. Y. K. Cheung 1976 *Finite Strip Methods in Structural Analysis*. Oxford: Pergamon Press.
14. S. S. Rao 1982 *The Finite Element Method in Engineering*. New York: Pergamon Press.
15. J. N. Reddy 1984 *An Introduction to the Finite Element Method*. New York: McGraw-Hill.
16. A. W. Leissa 1969 *Vibration of Plates* (*NASA SP 160*). Washington, D.C.: U.S. Government Printing Office.
17. G. B. Warburton 1954 *Proceedings of the Institution of Mechanical Engineers* **168**, 371–384. The vibration of rectangular plates.
18. A. W. Leissa 1973 *Journal of Sound and Vibration* **31**, 257–293. The free vibration of rectangular plates.
19. A. W. Leissa, P. A. A. Laura and R. H. Gutierrez 1979 *Journal of Applied Mechanics* **47**, 891–895. Vibration of rectangular plates with non-uniform elastic edge supports.
20. Y. K. Cheung and M. S. Cheung 1971 *Proceedings of the American Society of Civil Engineering Journal of the Engineering Mechanics Division* **97**, 391–411. Flexural vibration of rectangular and other polygonal plates.
21. M. S. Cheung 1971 *Ph.D. Thesis*, *University of Calgary*. Finite Strip Analysis of Structures.
22. S. C. Fan and Y. K. Cheung 1984 *Journal of Sound and Vibration* **93**, 81–94. Flexural free vibrations of rectangular plates with complex support conditions.
23. Y. Narita 1981 *Journal of Sound and Vibration* **77**, 345–355. Application of a series-type method to vibration of orthotropic rectangular plates with mixed boundary conditions.
24. P. A. A. Laura and R. H. Gutierrez 1994 *Journal of Sound and Vibration* **173**, 702–706. Analysis of vibrating rectangular plates with nonuniform boundary conditions by using the differential quadrature method.
25. C. Shu and C. M. Wang 1997 *International Journal of Solids and Structures* **34**, 819–835. Implementation of clamped and simply supported boundary conditions in the GDQ free vibration analysis of beams and plates.
26. C. Shu and C. M. Wang 1999 *Engineering Structures* **21**, 125–134. Treatment of mixed and nonuniform boundary conditions in GDQ vibration analysis of rectangular plates.
27. G. W. Wei 1999 *Journal of Chemical Physics* **110**, 8930–8942. Discrete singular convolution for the solution of the Fokker–Planck equations.
28. G. W. Wei 2000 *Journal of Physics A*: *Mathematical and General* **33**, 4935–4953. A unified approach for the solution of the Fokker–Planck equations.
29. L. Schwarz 1951 *Théore des Distributions*. Paris: Hermann.
30. G. W. Wei 2000 *Journal of Physics B* **33**, 343–352. Solving quantum eigenvalue problems by discrete singular convolution.
31. G. W. Wei 2000 *Computer Methods in Applied Mechanics and Engineering* **190**, 2017–2030. A new algorithm for solving some mechanical problems.
32. G. W. Wei 2000 *Physica D* **137**, 247–259. Discrete singular convolution method for the sine-Gordon equation.

33. M. J. Ablowitz, B. M. Herbst and C. Schober 1996 *Journal of Computational Physics* **126**, 299–314. On numerical solution of the sine-Gordon equation.
34. S. Guan, C.-H. Lai and G. W. Wei 2001 *Physica D* **151**, 83–98. Fourier–Bessel characterization of patterns in a circular domain.
35. G. W. Wei 1999 in *Computational Mechanics for the next Millennium* (C. M. Wang, K. H. Lee and K. K. Ang, editors), pp. 1049–1054. A unified method for computational mechanics, New York: Elsevier.
36. G. W. Wei 2001 *Journal of Sound and Vibration* **244**, 535–553. Vibration analysis by discrete singular convolution.
37. G. W. Wei 2001 *Engineering Structures* **23**, 1045–1053. Discrete singular convolution for beam analysis.
38. L. W. Qian and G. W. Wei 1999 *Journal of Approximation Theory* (submitted). A note on regularized Shannon's sampling formulae.
39. J. R. Wu and W. H. Liu 1988 *Journal of Sound and Vibration* **123**, 103–113. Vibration of rectangular plates with edge restraints and intermediate stiffeners.
40. A. H. Sheikh and M. Mukhopadhyay 1993 *Journal of Vibration and Acoustics* **115**, 295–302. Transverse vibration of plate structures with elastically restrained edges by the spline/finite strip method.